Infrared and optical properties of Na, K, and Rb metals

A. J. Sievers

Laboratory of Atomic and Solid State Physics and Materials Science Center, Cornell University, Ithaca, New York, 14853

(Received 4 March 1980)

The infrared and optical data on Na, K, and Rb are reanalyzed within the framework of the nearly-free-electron model with interband transitions and are shown to be inconsistent with this model. An intrinsic surface plasmon-assisted absorption process is proposed and the general frequency-dependent properties of this model are found to be consistent with experiment. When a detailed phenomenological description of this scattering process is incorporated into the nearly-free-electron model, the frequency dependences of both the optical conductivity and infrared mass data for solid alkali-metal–dielectric interfaces and of liquid Na are reproduced.

I. INTRODUCTION

The optical properties of the alkali metals have been measured many times over the last two decades.[1-3] Much of the early stimulus was provided by the work of Mayer and coworkers,[4,5] who found in bulk samples an additional absorption anomaly at frequencies smaller than the optical feature associated with interband transitions. Although recent measurements[6] seem to indicate that this extra absorption feature is activated by a surface film of metal-OH, a satisfactory mechanism has not yet appeared. In thick alkali-metal films, anomalous absorption bands at frequencies slightly larger than those associated with interband transitions have been identified either with the direct optical excitation of surface plasmons[7,8] due to surface roughness or with plasma resonances in the grain boundaries.[9] Surprisingly, the experimental studies of free-alkali-metal surfaces have not as yet shown consistent results.[3] The experimental situation is somewhat better for alkali-metal–dielectric interfaces, where recent experiments on Na-glass interfaces[10] have reproduced the earlier measurements by Smith,[11] in which a single feature in the optical conductivity of Na was identified with interband transitions.

The measured optical conductivity of Na-dielectric interfaces is shown in Fig. 1. The measurements on an Na-glass interface by Smith[11] (solid circles) were not reproduced for an Na-sapphire interface by Palmer and Schnatterly[8] (open circles), but recent measurements on Na-glass interfaces by Inagaki *et al.*[10] (open squares) have reconfirmed Smith's measurements. Also shown in Fig. 1 is the optical conductivity measured by Hietel and Mayer[12] (open triangles) for an Na-vacuum interface. The reason for the shifts in the peak position of the optical feature in Fig. 1 has remained an open question. The good agreement between the two sets of data for an Na-glass interface suggests that the optical data obtained by Smith for the other alkali metals[11,13] are reasonably accurate; the discrepancies with the other dielectrics suggests that the dielectric constant of the insulator contributes to the frequency of the optical feature.

In this paper, the alkali-metal–dielectric interface data are reexamined. The more complete experimental results now available on sodium are used to show that absorption processes based on interband transitions do not provide a consistent

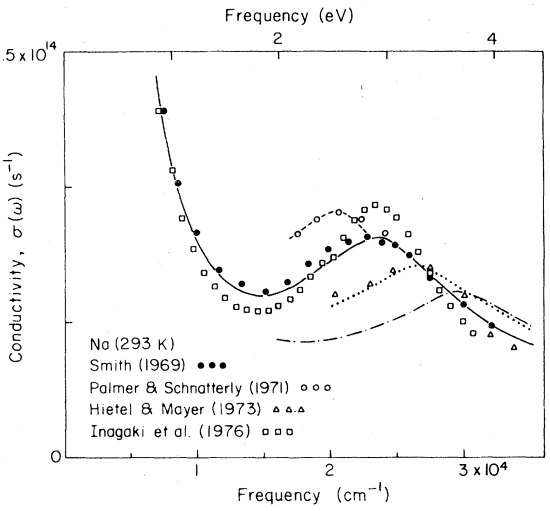

FIG. 1. The optical conductivity of Na-dielectric interfaces versus frequency. The experimental data are identified in the figure. The data by Smith and Inagaki *et al.* are for Na-glass interfaces ($\epsilon_D = 2.16$) while the data by Palmer and Schnatterly are for an Na-sapphire interface ($\epsilon_D = 3.15$). The data by Hietel and Mayer are for an Na-vacuum interface ($\epsilon_D = 1$). The different curves are described in Sec. III. The solid curve shows the surface-plasmon–assisted absorption fit to Smith's data. The model parameters are given in Tables I and II. The dashed curve is for the same parameters but with ϵ_D changed from 2.16 to 3.15. The dotted curve is for the same parameters but with ϵ_D changed from 2.16 to 1.5. Finally, the dot-dash curve is for the same parameters but with a vacuum interface.

description of the optical conductivity *and* the infrared mass. Analysis of Smith's data[11,13] on the other alkali metals supports this conclusion. It is next proposed that the observed peak in the optical conductivity is caused by an intrinsic surface-plasmon–assisted absorption which occurs at smooth metal surfaces. It is a Holstein-type process[14] with surface plasmons taking the role of phonons. A phenomenological model based on this idea is shown to be consistent both with the optical conductivity and the infrared mass data.

In Sec. II, the notation is defined, the optical properties of the nearly-free-electron (NFE) model with interband transitions are reviewed and compared with the experimental data. The discrepancy between the frequency dependence of the experimental infrared mass and the model is made apparent. To form a basis for the surface-plasmon model, Sec. II concludes with a review of the frequency-dependent electron-phonon relaxation time for a metal at absolute zero temperature.

The surface-plasmon–assisted process is described in Sec. III. Surface plasmons are introduced and the electron surface-plasmon relaxation time is calculated with a Debye model for surface plasmons. The frequency dependence of the renormalized electron mass follows directly from the frequency dependence of the relaxation time. A specific model for the surface which keeps track of the surface-plasmon depth in the metal is used in a detailed comparison with the experimental results. With one model parameter, namely the strength of the electron surface-plasmon coupling, the frequency dependent of both the relaxation parameter and the mass parameter are found to be consistent with the experimental data on the optical properties of solid Na-, K-, and Rb- dielectric interfaces and also for a liquid Na-vacuum interface. The apparent discrepancies in the optical conductivity shown in Fig. 1 are resolved by this model.

In Sec. IV some additional evidence is presented which supports the surface-plasmon–assisted absorption process, and the implications with regards to the optical properties of other metals are considered briefly.

II. BACKGROUND INFORMATION

A. NFE model plus interband transitions

For the alkali metals both intraband and interband transitions are assumed to be important. When optical conduction arises from two more-or-less independent groups of carriers, i.e., intraband and interband, the appropriate first approximation is to add the optical conductivities of each group, so

$$\sigma(\omega) = \sigma_D(\omega) + \sigma_I(\omega). \tag{1}$$

The Drude free-carrier term is represented by $\sigma_D(\omega)$, which is characterized by two parameters: $\omega_p^2 = 4\pi Ne^2/m$, where N is the number density of carriers, e the electron charge, and m the bare optical band mass; and τ, the effective carrier-relaxation time. Values of these quantities for Na, K, and Rb at room temperature can be obtained from columns 3, 5, and 6 in Table I, $\sigma_I(\omega)$ is the interband optical conductivity, which will be discussed shortly.

At infrared and visible frequencies smaller than the plasma frequency, the electron mean free path for alkali metals at room temperature is less

TABLE I. Some physical constants of Na, K, and Rb at room temperature. The values are obtained from Ref. 33 unless otherwise specified.

Metal	ρ_m (g/cm^3)	N (10^{22}) (No./cm^3)	$\frac{r_s}{a_0}$	$\frac{m}{m_0}$ [a]	ρ ($\mu\Omega$ cm)	$\frac{\delta}{l}$	ϵ_∞	V_{110} [f] (eV)
Na	0.971	2.54	3.99	1.00	4.75 [4.51] [b]	1.1	1.06 [c] (1.13) [d]	0.3
K	0.87	1.34	4.94	1.02	7.19 [6.55] [b]	1.5	1.15 [e] (1.23) [d]	0.17
Rb	1.53	1.08	5.31	1.06	12.5 [11.8] [b]	2.5	1.25 [e] (1.28) [d]	0.21

[a] F. S. Ham, Phys. Rev. 128, 2524 (1962).

[b] The bracketed dc resistivity values gave the best low-frequency fit to the optical conductivity data of Smith.

[c] The value of ϵ_∞ discussed in J. C. Sutherland and E. T. Arakawa, J. Opt. Soc. Am. 57, 645 (1967).

[d] The values of ϵ_∞ used by Ref. 15.

[e] The values of ϵ_∞ measured in Ref. 28.

[f] Described in the text in Sec. II B.

than the classical skin depth $\delta = c/\omega_p$ (see column 7, Table I), so normal skin-effect conditions prevail. The imaginary part of the dielectric function is[15]

$$\epsilon_2(\omega) = \frac{\omega_p^2\tau^2}{(1+\omega^2\tau^2)}\left(\frac{1}{\omega\tau}\right) + \frac{4\pi\sigma_I(\omega)}{\omega} . \quad (2)$$

When $\omega\tau \gg 1$, the Drude electrons are thought to be scattered in two ways: (1) by phonons and (2) by the surface. The bulk relaxation time τ_b due to scattering by phonons can be obtained from the dc resistivity ρ and the electron density given in Table I. The surface scattering time τ_s due to diffuse scattering of the electrons colliding with the metal surface depends only on the electron density. The reciprocal relaxation times due to each component are added together to give the resultant relaxation frequency,[16] so

$$(\tau)^{-1} = (\tau_b)^{-1} + (\tau_s)^{-1} \quad (3)$$

which is a simple function of ρ, the electron density, and the optical mass. Since ρ and the electron density are known independently, only the optical mass is required to completely specify the Drude infrared reflectivity.[17]

The excitation of interband transitions at larger frequencies adds another degree of freedom to the optical conduction process. Early investigators fit these optical features with Lorentz oscillators,[18] but most recent studies have used the Wilson-Butcher expression[19,20] for $\sigma_I(\omega)$ which is given by Eq. (A1) in Appendix A. For the alkali metals, the threshold for the excitation of this degree of freedom occurs at $0.64E_F$, which is in reasonable agreement with the optical conductivity feature for Na, K, and Rb (Ref. 11). Somewhat better agreement with the exact frequency dependence of the optical conductivity has been obtained by Stevenson[21] who included phonon-assisted interband transitions to thermally broaden the threshold energy.

A complete representation of the real part of the dielectric function for the alkali metals in the infrared and optical region must include not only interband and Drude contributions but also a term associated with the dc polarizability of core electrons, usually defined as $4\pi N_0\alpha_0$. The resultant real part of the dielectric function is[15]

$$\epsilon_1(\omega) = \epsilon_\infty - \omega_p^2\tau^2/(1+\omega^2\tau^2) + \epsilon_{1I}(\omega) , \quad (4)$$

where $\epsilon_\infty = 1 + 4\pi N_0\alpha_0$ and $\epsilon_{1I}(\omega)$, the Kramers-Kronig transform[11] of $4\pi\sigma_I(\omega)/\omega$, is given by Eq. (A2) in Appendix A. In the infrared below the interband threshold but where $\omega\tau \gg 1$, Eq. (4) simplifies to

$$\epsilon_1(\omega) = \epsilon_\infty - \omega_p^2/\omega^2 + \text{const} \quad (5)$$

so the experimental optical mass can be determined from the slope of $\epsilon_1(\omega)$ vs ω^{-2} data. Another puzzle of the alkali-metal data has been that the measured infrared mass is larger than the measured optical mass at the interband threshold,[11,12] in contradiction with the predictions of Eqs. (2) and (4). A closer examination of this discrepancy will demonstrate the inconsistency of assuming that the optical constants are determined only by Drude-type absorption and interband transitions.

B. Comparison with experiment

To compare the experimentally measured frequency dependence of the mass with that predicted by the nearly-free-electron model including interband transitions, it turns out to be convenient to equate both the measured dielectric function and Eqs. (2) and (4) to a Drude model with frequency-dependent parameters $\tau(\omega)$ and $\omega_p(\omega)$. Because the Drude model with constant coefficients successfully describes the intraband process, the frequency dependence of the two parameters can be identified with the interband process. The two parameters are

$$1/\omega\tau(\omega) = \epsilon_2(\omega)/[\epsilon_\infty - \epsilon_1(\omega)] \quad (6)$$

and

$$\omega_p^2(\omega)/\omega^2 = \{\epsilon_2^2(\omega) + [\epsilon_\infty - \epsilon_1(\omega)]^2\}/[\epsilon_\infty - \epsilon_1(\omega)] , \quad (7)$$

where $\omega_p^2(\omega) = [m/m(\omega)]\omega_p^2$. The frequency dependence of the optical mass can be examined directly by defining a mass parameter $\lambda(\omega)$ so

$$\lambda(\omega) = [m(\omega)/m] - 1 . \quad (8)$$

Smith's dielectric functions,[11,13] together with the values of ϵ_∞ given in Table I, are used to calculate the experimental values of $[\omega\tau(\omega)]^{-1}$ and $\lambda(\omega)$. These experimental values are shown in Fig. 2 for Na, Fig. 3 for K, and Fig. 4 for Rb.

The NFE interband model values are found in a similar manner. The Drude contribution determines the low-frequency values of $[\omega\tau(\omega)]^{-1}$. The experimental ρ and theoretical optical masses listed in Table I produce reasonable agreement with the experimental $[\omega\tau(\omega)]^{-1}$; however, to obtain an exact fit to the low-frequency data the bracketed values of ρ in Table I have been used. The NFE interband model has one remaining parameter, the band-matrix element V_{110}. For each alkali metal, the magnitude of this coefficient has been evaluated from a fit to the optical conductivity data, then, with the alkali-metal parameters given in Table I, model values of $[\omega\tau(\omega)]^{-1}$ and $\lambda(\omega)$ are obtained.

The dashed curve in Fig. 2(a) shows the fit with the Wilson-Butcher model. The corresponding $\lambda(\omega)$ is represented by the dashed curve in Fig.

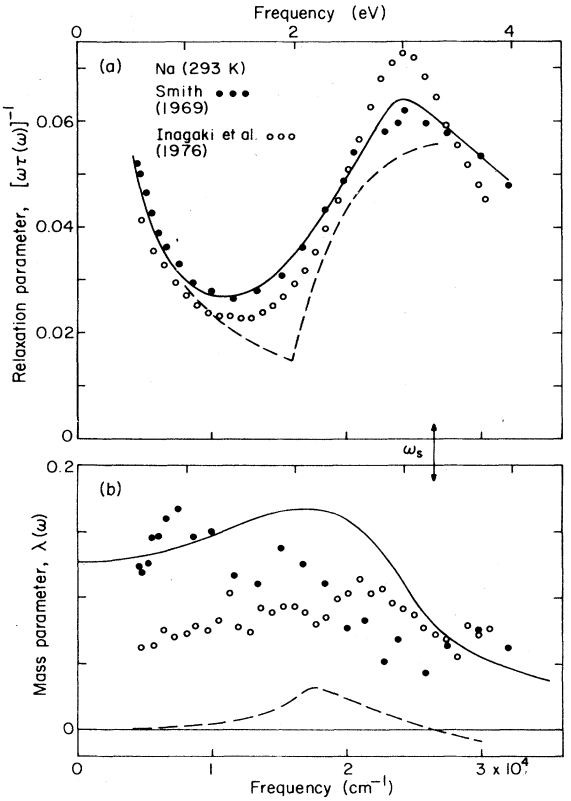

FIG. 2. (a) The relaxation parameter for an Na-glass interface versus frequency. The experimental data are identified in the figure. The dashed curve illustrates the fit to the Butcher-Wilson expression described in Sec. II. The model parameters are given in Table I. The solid curve is calculated using the surface-plasmon–assisted absorption model described in Sec. III. The model parameters are listed in Tables I and II. (b) The frequency-dependent mass parameter for an Na-glass interface versus frequency. The identification of the data and the solid and dashed curves are the same as in (a). For reference, the electrostatic surface-plasmon frequency ω_s is identified.

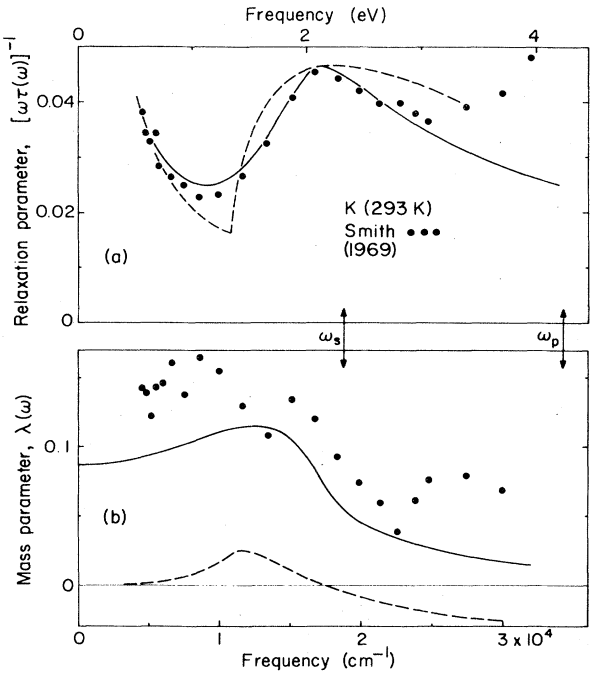

FIG. 3. (a) The relaxation parameter for a K-glass interface versus frequency. The experimental data are identified in the figure. The dashed curve illustrates the fit to the Butcher-Wilson expression described in Sec. II. The model parameters are given in Table I. The solid curve is calculated using the surface-plasmon–assisted absorption model described in Sec. III. The model parameters are listed in Tables I and II. (b) The frequency-dependent mass parameter for a K-glass interface versus frequency. The identification of the data and the solid and dashed curves are the same as in (a). For reference, the electrostatic surface-plasmon frequency ω_s and the bulk-plasmon frequency ω_p are identified.

2(b). Experimental results for Na are represented by the open and closed circles. The relative scatter in both sets of data demonstrates that the measurement of $\lambda(\omega)$ is somewhat less precise than the measurement of $[\omega\tau(\omega)]^{-1}$, nevertheless, it is still apparent that in Fig. 2(b) neither set of experimental data agree in magnitude or frequency dependence with the dashed curve.

Figures 3 and 4 show similar comparisons for K and Rb. In both cases V_{110} can be chosen so that the feature in the relaxation frequency (or optical conductivity) can be fit fairly well but again neither the magnitude nor the frequency dependence of $\lambda(\omega)$, as given by the interband [dashed curves in Figs. 3(b) and 4(b)], agree with the data.

How unique is the comparison in each figure? The frequency dependence of $\lambda(\omega)$ depends to some extent on the value of ϵ_∞, as can be seen by inspection of Eq. (6). At high frequencies, where $\epsilon_1(\omega)$ is small, the value of ϵ_∞ is important while at low frequencies, where $\epsilon_1(\omega)$ is large, the value of $\lambda(\omega)$ is independent of this parameter. In Ref. 15 slightly larger values of ϵ_∞ have been used (see Table I, column 8). Larger ϵ_∞'s decrease both the experimental and interband model $\lambda(\omega)$'s for frequencies larger than the interband threshold, which only increases the discrepancy between the frequency dependences of the experimental data and the interband model.

Stevenson[21] has shown that the NFE interband model can be brought into better agreement with the optical conductivity data of Smith if phonon-assisted interband transitions are also included. The thermal energy broadens the sharp threshold characteristic of the Wilson-Butcher model but the direct interband transitions remain the dominant

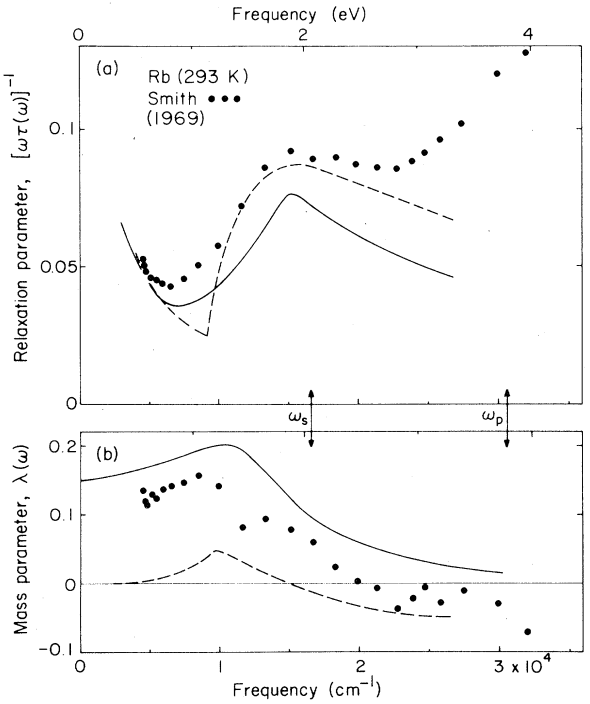

FIG. 4. (a) The relaxation parameter for an Rb-glass interface versus frequency. The experimental data are identified in the figure. The dashed curve illustrates the fit to the Butcher-Wilson expression described in Sec. II. The model parameteres are given in Table I. The solid curve is calculated using the surface-plasmon–assisted absorption model described in Sec. III. The model parameters are listed in Tables I and II. (b) The frequency-dependent mass parameter for an Rb-glass interface versus frequency. The identification of the data and the solid dashed curves are the same as in (a). For reference, the electrostatic surface-plasmon frequency ω_s and the bulk-plasmon frequency ω_p are identified.

process. Hence, although the Drude conductivity and phonon-assisted interband conductivity are no longer additive because of interference terms, this thermal modification can not qualitatively alter the dashed curves in Figs. 2(b), 3(b), and 4(b), because most of the strength at frequencies larger than the threshold is still associated with the direct processes, hence, as $\omega \to 0$ then $\lambda(\omega) \to 0$. The added conductivity associated with the excitation of a second set of carriers at finite frequencies (interband transitions) does not provide a low-frequency mass enhancement. This discrepancy in the infrared mass parameter indicates that another mechanism must also contribute to the optical absorption in alkali metals.

C. Holstein effect

Holstein[14] first showed that, at absolute zero temperature, the consequence of linear coupling between electrons and phonons was a frequency-dependent relaxation time and a mass enhancement for frequencies smaller than the maximum phonon frequency. The conduction electrons are able to absorb a photon in this purely bulk process because phonon emission allows for the conservation of both momentum and energy. At the maximum phonon frequency there are many more phonons that can take up the momentum differences between the incident photons and electrons than at lower frequencies, hence the relaxation time decreases with increasing frequency.

The phonon-assisted relaxation time has been calculated within the golden-rule approximation by Allen.[22] To calculate the ac conductivity, the perturbation Hamiltonian is taken to have two parts, the radiation field part $H_{\rm ext}$, and the electron-phonon part $H_{\rm ep}$, which are defined as follows:

$$H_{\rm ext} = \sum_{\vec{k}} \frac{e}{c} (\vec{v}_{\vec{k}+\vec{q}/2}) \cdot \vec{A}_{\rm ext} c^{\dagger}_{\vec{k}+\vec{q}} c_{\vec{k}} , \tag{9}$$

where $c^{\dagger}_{\vec{k}}$ is the creation operator for a Bloch electron of wave vector $\vec{k}$, of energy $\epsilon_{\vec{k}}$, and velocity $\vec{v}_{\vec{k}}$, and $\vec{A}_{\rm ext}$ is the vector potential of the radiation field;

$$H_{\rm ep} = \sum_{\vec{k}\vec{k}'} M_{\vec{k}\vec{k}'} c^{\dagger}_{\vec{k}'} c_{\vec{k}} (a_{\vec{Q}} + a^{\dagger}_{-\vec{Q}}) , \tag{10}$$

where $M_{\vec{k}\vec{k}'}$ is the matrix element for scattering an electron from a Bloch state $\vec{k}$ to $\vec{k}'$ by electron-phonon scattering, and $a^{\dagger}_{\vec{Q}}$ is the creation operator for a phonon of wave vector $\vec{Q} = \vec{k}' - \vec{k}$ and energy $\hbar\Omega_{\vec{Q}}$. Phonon polarization, electron band, and spin indices are suppressed. A calculation of the optical conductivity in the limit $\omega\tau(\omega) \gg 1$ gives[22]

$$[\omega\bar{\tau}(\omega)]^{-1} = \frac{2\pi}{\omega^2} \int_0^{\omega} d\Omega(\omega - \Omega)\alpha^2_{\rm ir} F(\Omega) , \tag{11}$$

where $\alpha^2_{\rm ir} F(\Omega)$ is the phonon density of states weighted by the amplitude for large-angle scattering on the Fermi surface. For frequencies small compared to the maximum phonon frequency, the relaxation parameter is

$$[\omega\bar{\tau}(\omega)]^{-1} \sim \omega^4 , \tag{12}$$

and it is a constant value for frequencies larger than the maximum phonon frequency. The mass parameter $\bar{\lambda}(\omega)$, which is intimately related to the Kramers-Kronig transform of $[\omega\bar{\tau}(\omega)]^{-1}$ is given in Appendix B.

The physical interpretation of this frequency-dependent mass is as follows: At frequencies large compared to the phonon frequencies, the polarization cloud associated with the phonons cannot follow the electrons so the electrons have their bare optical mass $[\lambda(\omega) \to 0]$, while at small frequencies the polarization cloud does follow the electrons and the mass enhancement of the

electrons results [$\lambda(0) \neq 0$]. Although the actual observation of this effect in metals at low temperatures is often masked by Landau damping (the anomalous skin effect), the example demonstrates that frequency-dependent relaxation processes acting on a given group of carriers cause a low-frequency mass enhancement for these carriers. Phonon energies are too small to account for the infrared-mass enhancement of the alkali metals, however.

III. SURFACE-PLASMON-ASSISTED ABSORPTION

A. Surface plasmons

To derive the dispersion relation for surface plasmons on a metallic half-space bounded by vacuum valid in a region where retardation effects are important, all of Maxwell's equations are needed as well as the usual boundary conditions on the electric and magnetic fields. For a vacuum-bounded electron gas the transverse magnetic (TM) polarized surface wave dispersion relation is $\omega = c\kappa$, as $\kappa \to 0$, and the excitation outside of the metal is almost completely transverse in character. As κ increases, ω increases monotonically to the asymptotic value $\omega_s = \omega_p/\sqrt{2}$, at which point the excitation is almost completely longitudinal in character.[23]

More generally, if the dielectric function of the metal is $\tilde{\epsilon}_m(\omega)$ and the dielectric constant of the remaining half-space is ϵ_d, then the dispersion relation for the surface wave is[24]

$$\tilde{\kappa}^2 = \frac{\omega^2}{c^2}\left(\frac{\tilde{\epsilon}_m(\omega)\epsilon_d}{\tilde{\epsilon}_m(\omega)+\epsilon_d}\right), \tag{13}$$

where $\tilde{\kappa}$ is the complex wave vector parallel to the surface. The high-frequency asymptotic limit to this dispersion curve occurs when $\tilde{\epsilon}_m(\omega) = -\epsilon_d$, giving the electrostatic surface-plasmon frequency

$$\omega_s^2 = \omega_p^2/(\epsilon_\infty + \epsilon_d), \tag{14}$$

where ϵ_∞ includes the contribution from the core electrons. At low frequencies $|\tilde{\epsilon}_m(\omega)| \to \infty$, so

$$\kappa^2 \to \epsilon_d \omega^2/c^2. \tag{15}$$

At a given frequency, κ of the surface plasmon is always larger than the k vector of the bulk radiation. Electromagnetic radiation, therefore, cannot couple directly to these modes at a plane metal surface since energy and momentum cannot both be conserved.

In contrast with bulk plasmons, some surface plasmons are excited at room temperature. At a temperature T, the mean surface-plasmon occupation number is

$$n(\kappa) = \{\exp[\beta\hbar\omega(\kappa)] - 1\}^{-1}. \tag{16}$$

At all reasonable temperatures, appreciable excitation occurs for $\omega(\kappa) \ll \omega_s$, the dispersion curve is linear, the surface-plasmon density of states is

$$F(\omega) \cong (\epsilon_d/2\pi)\omega/c^2, \tag{17}$$

and the energy density of these modes is described by a two-dimensional blackbody spectrum. In what follows, these thermally excited surface plasmons will be ignored because, for the alkali metals, $\hbar\omega_s$ and $\hbar\omega$ are much greater than kT.

B. Electron-surface-plasmon relaxation time

1. Homogeneous medium approximation

In this section an analogy is drawn between the phonon-assisted absorption described by Holstein and a surface-plasmon–assisted process.

A correct description of the dynamics of even the simplest smooth metal surface should involve not only quasiparticles and retarded surface plasmons, but also (because the two kinds of excitations are not completely orthogonal) the interaction between them. The perturbation Hamiltonian for a calculation of the optical conductivity is taken to have two parts: the radiation field part H_{ext}, given by Eq. (9), and the electron-surface plasmon part H_{esp}. This latter term can be written as

$$H_{\text{esp}} = \sum_{\vec{k}} \frac{e}{c}(\vec{v}_{\vec{k}+\vec{\kappa}/2}) \cdot \vec{A}_{\text{sp}} c^\dagger_{\vec{k}+\vec{\kappa}} c_{\vec{k}}, \tag{18}$$

where $\vec{v}_{\vec{k}}$ is the Bloch electron velocity and where $\vec{A}_{\text{sp}}$ is the vector potential of the surface-plasmon field.[25] Its specific form is given in Appendix C. Of importance here is that $\vec{A}_{\text{sp}}$ is linear in the surface-plasmon creation and annihilation operators, hence, H_{esp} has the same form as H_{ep} in Eq. (10).

An important quantity for characterizing the surface-plasmon–assisted absorption process is the depth $\Delta(\omega)$ of the surface-plasmon excitation within the metal,

$$\Delta(\omega) = (\text{Im}\tilde{\kappa}_{\perp m})^{-1}, \tag{19}$$

where $\tilde{\kappa}_{\perp m}$ signifies the complex κ vector in the metal perpendicular to the surface, and

$$\tilde{\kappa}^2_{\perp m} = (\omega/c)^2[\tilde{\epsilon}_m(\omega)]^2/[\tilde{\epsilon}_m(\omega) + \epsilon_d]. \tag{20}$$

At infrared frequencies with $\omega\tau \gg 1$, $\Delta(\omega)$ reduces to the classical skin depth $\delta = c/\omega_p$, which is greater than the electron mean free path l. Since the optical excitation and surface-plasmon excitation are confined to the same region in space, the optical relaxation time for the scattering of a conduction electron which simultaneously absorbs a photon and emits a surface plasmon can be obtained with the formalism developed to describe the electron-phonon effects. At optical frequencies

this picture breaks down.

When $\mathrm{Re}(\tilde{\epsilon}_m) \to -\epsilon_d$, then $\Delta(\omega) < l < \delta$. The surface-plasmon–electron interaction passes into the anomalous-skin-effect regime while the electron-photon interaction remains in the normal-skin-effect limit. Only a fraction of the electrons within the surface-plasmon depth Δ, namely that fraction Δ/l which spends its entire mean free path there, can interact with the surface plasmons. Although at low frequencies the relative fraction of the interacting electrons within the fields of both kinds of excitations is Δ/δ, at optical frequencies, near ω_s, the relative fraction is $\Delta^2/l\delta$. At the frequency ω_s, just where the peak in the surface-plasmon density occurs, only a very small fraction of the electrons which interact with the electromagnetic radiation can interact with the surface plasmons. Because of the expected near-cancellation of the singularity in the density of surface-plasmon states with the singularity in the effective number of interacting electrons [compare Eqs. (13) and (20)], the interacting surface plasmons can be approximated by a linear dispersion curve over the entire frequency interval with a cutoff at some maximum frequency ω_m, which is approximately equal to ω_s [see Eq. (14)] but is still to be determined. The density of these surface-plasmon states, which is given by Eq. (17) for $\omega \leq \omega_m$ and by $F(\omega) = 0$ for $\omega > \omega_m$, is used in the calculation of the surface-plasmon–assisted optical relaxation time.

The surface-plasmon density of states weighted by the amplitude for large-angle scattering (ω^2) on the Fermi surface is

$$\alpha_{\mathrm{ir}}^2 F(\omega) = \left(\frac{\epsilon_d}{2\pi}\frac{\omega}{c^2}\right)\left(\frac{\omega_p}{c}\right) S\omega^2 , \tag{21}$$

where S represents a frequency-independent coupling constant and $\delta = c/\omega_p$, the important length in the problem, is introduced to give the function the same dimensions as in the electron-phonon problem. Then, by Eq. (11), the relaxation parameter is

$$[\omega\bar{\tau}(\omega)]^{-1} = \frac{S}{20}\,\epsilon_d\,\frac{\omega_p}{c}\,\frac{\omega^3}{c^2} \quad \text{for } \omega \leq \omega_m \tag{22}$$

and is constant for $\omega > \omega_m$. The notation can be simplified somewhat by rewriting Eq. (22) as

$$[\omega\bar{\tau}(\omega)]^{-1} = [\omega_m\bar{\tau}(\omega_m)]^{-1}(\omega/\omega_m)^3 . \tag{23}$$

The corresponding expression for $\bar{\lambda}(\omega)$ is given by Eq. (B2) in Appendix B. The frequency dependence of $\bar{\lambda}(\omega)$ is closely related to the frequency dependence of the Kramers-Kronig transform of $[\omega\bar{\tau}(\omega)]^{-1}$, which is given by Eq. (B4) in Appendix B.

The two frequency-dependent Drude-model parameters $\omega_p(\omega)$ and $\tau(\omega)$ are given by[22]

$$[\omega_p(\omega)]^2 = \omega_p^2/[1+\bar{\lambda}(\omega)] \tag{24}$$

and

$$\tau(\omega) = \bar{\tau}(\omega)[1+\bar{\lambda}(\omega)] . \tag{25}$$

Note that the mass renormalization parameter does not explicitly appear in the dc conductivity,

$$\sigma_{\mathrm{dc}} = \omega_p^2\bar{\tau}(0)/4\pi . \tag{26}$$

2. *Composite medium relaxation time*

So far, the phenomenological relaxation time contains two parameters, the coupling strength S and the maximum frequency of the effective plasmons ω_m. This latter parameter can be related to the electron density by making use of a physical model which keeps track of the surface-plasmon depth $\Delta(\omega)$ in the metal.

The metal half-space is divided into two layers: an outer film of thickness $\Delta(\omega)$ which contains surface-plasmon scattering and an inner half-space which represents the bulk metal. This division should be a reasonable approximation since the nonlocal effects expected at optical frequencies have already been taken into account by means of the effective dispersion curve introduced earlier. Next, the intensity of radiation reflected from this composite is calculated.

In general, the intensity of radiation reflected from an absorbing layer on top of a second absorbing medium is quite intricate because of interference effects; however, if both media are metallic, with the bulk metal characterized by Drude parameters ω_p and τ, and the surface film by ω_p and $\{(\tau)^{-1}+[\bar{\tau}(\omega)]^{-1}\}$, and if $\omega\tau$, $\omega\bar{\tau}(\omega) \gg 1$, then the absorptivity $A(\omega)$ has a particularly simple form:

$$A(\omega) = \frac{2}{\omega_p}\left(\frac{1}{\tau} + \frac{1}{\bar{\tau}(\omega)}\left(1 - e^{-\beta(\omega)}\right)\right) \equiv \frac{2}{\omega_p\tau_c(\omega)} , \tag{27}$$

where τ_c is the effective relaxation time of the composite structure. For the infrared and optical region, $\beta(\omega) = 2\Delta(\omega)/\delta$.

τ_c has the correct physical limits: At low frequencies $\bar{\tau}(\omega)$ dominates and the relaxation frequency increases over that of the bulk as ω^4 while at ω_s, $\beta \to 0$ and the relaxation frequency decreases towards the bulk value. The optical frequency between these two limits which produces the maximum $[\tau_c(\omega)]^{-1}$ is identified with ω_m, now only a function of the electron density and the dielectric constant ϵ_d.

To make contact with the frequency-dependent Drude model represented by Eqs. (24) and (25), the $\tau_c(\omega)$ in Eq. (27) is identified with $\bar{\tau}(\omega)$ in Eq. (25). To obtain a consistent value of the frequency dependence of the mass parameter $\lambda_c(\omega)$, a numerical evaluation of the Kramers-Kronig trans-

form of $[\omega\tau_c(\omega)]^{-1}$ must be performed,

$$\frac{\lambda_c(\omega)}{2.5} = \frac{2}{\pi} P \int_0^\infty \frac{[\tau_c(u)]^{-1}}{u^2 - \omega^2} du , \tag{28}$$

where the scale factor of 2.5 is obtained from Eq. (B5) in Appendix B. This value of $\lambda_c(\omega)$ is identified with $\bar{\lambda}(\omega)$ in Eqs. (24) and (25).

C. Comparison with experiment

A cursory examination of the data in Figs. 2–4 shows a general consistency with the model just presented. From Appendix B, Eq. (B3), the model predicts that $\lambda_c(0) \approx 2[\omega_m \tau_c(\omega_m)]^{-1}$, i.e., the peak value of the relaxation parameter is one-half the value of the low-frequency mass parameter. Indeed, the peak values of the feature in Figs. 2(a), 3(a), and 4(a) is roughly one-half of the infrared-mass parameters in Figs. 2(b), 3(b), and 4(b). A more quantitative comparison is made below.

According to Sec. III B 2, the relaxation time $\tau_c(\omega)$ is a function of the electron density N, the dc resistivity ρ, the dielectric constant of the insulating half-space ϵ_d, the bare optical band mass m, and the coupling constant S. The first three of these quantities can be obtained from Table I. In the absence of interband transitions but with surface-plasmon coupling present, the bare optical band mass should correspond to the experimentally measured mass for frequencies large compared to the optical feature. The high-frequency experimental masses listed in Table II are in good agreement with the theoretical values of the optical mass listed in Table I, and it is these experimental values which are used in the comparisons below. The one parameter which remains, S, is fit to the experimental relaxation-parameter data given in Figs. 2(a), 3(a), and 4(a). The solid curves in these figures show such a fit to Smith's data with the values of $[\omega_m \tau_c(\omega_m)]^{-1}$ listed in Table II. Note that the frequency position of this anomaly, ω_m, which is also listed in Table II, is independent of S. With S (or, equivalently, $[\omega_m \tau_c(\omega_m)]^{-1}$) fixed, $\lambda_c(\omega)$ is completely determined. These calculated values are represented by the solid curves in Figs. 2(b), 3(b), and 4(b). In each case, the agreement with experiment is encouraging.

TABLE II. Physical parameters of Na, K, and Rb used in Sec. III.

Metal	$\frac{m}{m_0}$	$\frac{r_s}{a_0}$ (opt)	$\hbar\omega_m(\epsilon_D)$ (eV)	$[\omega_m\tau_c(\omega_m)]^{-1}$
Na (293 K)	[1.01] [a]	4.00	3.88(1)	0.06
			3.46(1.5)	0.06
			3.09(2.16)	0.06
			2.69(3.15)	0.06
Na (393 K)	[1.01] [a]	4.05	3.81(1)	0.05
K (293 K)	1.01 [b]	4.96	2.19(2.16)	0.05
Rb (293 K)	1.03 [b]	5.36	1.93(2.16)	0.08

[a] Reference 16 found the optical mass of Na and K to be the same so the value for K from Ref. 28 is used.
[b] Reference 28.

According to the model, the dc resistivity determines the product of the bare optical band mass and the bare relaxation time (see Eq. 26). The experimental dc resistivities listed in Table I provide good agreement (the solid curves) with the experimental relaxation parameter at low frequencies below the optical feature in Figs. 2(a), 3(a), and 4(a). For the interband plus Drude model, it was found in Sec. II that a dc resistivity value (see bracketed values in Table I) different from the measured dc value was required to fit the low-frequency data (dashed curves).

For the surface-plasmon–assisted process, the frequency position of the optical feature ω_m should depend on ϵ_d. The most complete experimental results for different ϵ_d's have been on Na-dielectric interfaces. These data have already been presented in Fig. 1 and this figure is now examined in more detail. The model conductivity which fits the Na-glass interface data in Fig. 2 is represented by the solid curve in Fig. 1. When ϵ_d is changed from 2.16 (glass) to 3.15 (sapphire) the solid curve in Fig. 1 shifts to the dashed curve. Both the relative magnitude and frequency position of the optical anomaly are consistent with the experimental data.

Also shown in Fig. 1 is the free-Na-surface data of Hietel and Mayer,[12] where a weaker anomaly at larger frequencies is observed. Replacing $\epsilon_d = 3.15$ by $\epsilon_d = 1.0$ shifts the model curve from the dashed to the dot-dashed one. The agreement is less clear than for the dielectric interface results; however, it has been reported[6] that these surfaces are covered with a metal-OH overlayer. Such an overlayer would give rise to an effective $\epsilon_d > 1$, the exact value depending on the overlayer thickness, which would shift the feature in the dot-dash curve to lower frequencies. Choosing $\epsilon_d = 1.5$ gives the dotted curve in Fig. 1, which is in good agreement with the data. A more detailed comparison with the experimental measurements of the free alkali-metal surfaces has not been pursued because, in addition to overlayers, there are experimental problems associated with surface roughness.[7,8]

Liquid alkali metals represent another system where the surface-plasmon model can be tested, since the surface will be smooth and, in addition, interband transitions should not occur. Early measurements on liquid metals did show structure in the optical conductivity,[4,5] but because of the

possible ambiguities introduced by metal-OH overlayers[6] these measurements will not be discussed here. However, new measurements by Inagaki *et al.*[26] on a clean liquid-Na surface still reveal structure in the optical conductivity and an infrared mass enhancement. The experimental data points are represented by the open squares in Fig. 5. Given the electron density and dc resistivity values of liquid Na and for S(liquid)/S(solid) $=0.8$, the model gives the two solid curves. Although the model qualitatively accounts for both optical and infrared anomalies, a quantitative comparison cannot be made because the liquid surface measurements are less accurate than the Na-glass interface work.

IV. DISCUSSION AND CONCLUSIONS

General features of the surface-plasmon–assisted absorption process which are independent of the details of the scattering model can be seen in the experimental data. The process depends on the dielectric constant of the insulating overlayer because the surface plasmon has an inhomogeneous electromagnetic field associated with it which extends into the dielectric. The surface excitations in the metal give rise to an intrinsic scattering process for quasiparticles near the surface and it is just these quasiparticles which are probed by optical radiation. Due to surface-plasmon emission, the relaxation parameter varies as ω^3 at low frequencies because the surface-plasmon density of states ($\sim\omega$) is weighted by the usual $(1-\cos\theta)$ factor ($\sim\omega^2$) since large-angle-scattering processes are most important. For frequencies larger than the electrostatic surface-plasmon frequency ω_s, (which is determined by the electron density and ϵ_d), no new scattering processes can occur and the relaxation time is frequency independent. Associated with the frequency-dependent scattering process is a renormalization of the optical mass of the surface quasiparticles at low frequencies. Each quasiparticle when it enters the surface region creates a cloud of retarded surface plasmons, some of which propagate away but most of which remain with the particle and follow its motion at infrared frequencies. This cloud cannot follow the motion of the particle above optical frequencies. For a quasiparticle to reenter the bulk, it must reabsorb a "complete" cloud of surface plasmons. Because the energies involved are much greater than kT, some of these surface plasmons must be supplied by nearby quasiparticles entering the surface. Hence, the quasiparticle motion into and out of the surface region must be strongly correlated. Other implications of electron-electron coupling with electrostatic surface plasmons have been considered by Inkson.[27]

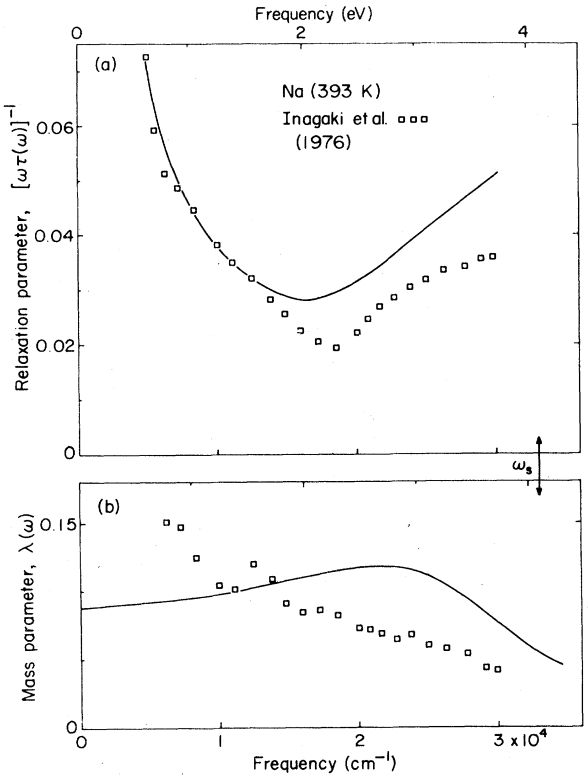

FIG. 5. (a) The relaxation parameter for liquid Na versus frequency. The experimental data are identified in the figure. The solid curve is calculated using the surface-plasmon–assisted absorption model described in Sec. III. The dc resistivity is taken as 10.6 $\mu\Omega$ cm and the other model parameters are listed in Table II. (b) The frequency-dependent mass parameter for liquid Na versus frequency. The identification of the data and the solid curve are the same as in (a). For reference, the electrostatic surface-plasmon frequency, ω_s is identified.

There is additional circumstantial evidence at larger frequencies which supports the surface-plasmon–assisted absorption model. The measured optical constants for potassium over a large frequency region,[11,28] reexpressed in terms of the relaxation parameter and the mass parameter, are shown in Fig. 6. The feature in the relaxation parameter near ω_s, which is the subject of this paper, is completely dominated by a second feature near $2\omega_p$. Inspection of the frequency-dependent signatures of the mass parameter in Fig. 6(b) illustrates that the two features have very different origins. Near $2\omega_p$, the mass parameter is both negative and positive, with a maximum positive value which is much smaller than the maximum value of $[\omega\tau(\omega)]^{-1}$ in Fig. 6(a). The similarity in frequency dependence between the high-frequency data shown in Fig. 6(b) and the dashed curve in

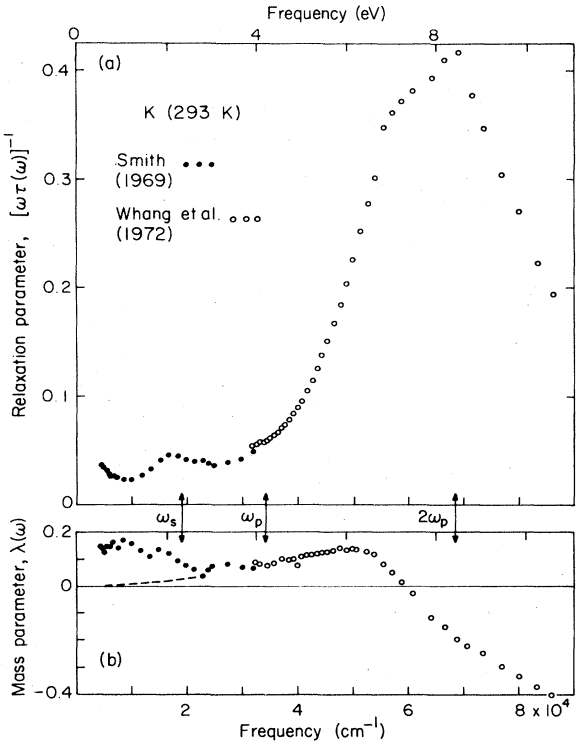

FIG. 6. (a) The relaxation parameter for K-glass interface versus frequency. The experimental data which are identified in the figure show that two features occur, one near ω_s and one near $2\omega_p$. (b) The frequency-dependent mass parameter for a K-glass interface versus frequency. The identification of the data is the same as in (a). The measured frequency dependence of the mass parameter illustrates that the two optical features have different origins. The one near $2\omega_p$ is associated with the excitation of a new degree of freedom (perhaps two-plasmon absorption) while the one near ω_s is associated with frequency-dependent scattering of the single-particle excitations. The dashed line is a guide to the eye.

Fig. 3(b) is striking. This frequency dependence of the mass parameter with its characteristic change in sign is indicative of the excitation of a new degree of freedom, hence, the optical conductivity of this process should be added to the optical conductivity of the low-frequency process to obtain the total conductivity. The dashed line in Fig. 6(b) is a guide to the eye and represents a natural extension to zero frequency of the frequency-dependent mass parameter for the process near $2\omega_p$.

Although previously this feature has been assigned to interband transitions,[29] it should be noted that room temperature is 0.9 of the melting temperature of potassium. The frequency position $2\omega_p$ is also consistent with a two bulk-plasmon absorption process where the excited plasmons have equal and opposite momenta. The large width would follow from the strong electron-electron damping of plasmon waves with large k vectors.

The frequency signature of the remaining mass parameter at low frequencies is consistent with intraband carriers not only involved in frequency-independent scattering from phonons and the metal surface, but also a frequency-dependent scattering due to the interaction with surface plasmons. The measured optical constants show that a new degree of freedom is not excited in the infrared or optical region.

Since the current analysis of the infrared and optical properties of the alkali metals represents an obvious departure from past explanations, a few remarks should be made with regard to the optical properties of other metals. All the alkali metals treated here satisfy the weak electron–surface-plasmon coupling condition $[\omega_m\tau(\omega_m)]^{-1} \ll 1$. From Table II it is seen that the coupling is stronger for Rb than for Na or K. The large infrared mass of Cs measured by Smith[13] suggests that an even stronger coupling exists for Cs than for Rb, so that the weak-coupling phenomenological model described here no longer applies. These results may indicate that the coupling strength is related to the screening length which is inversely related to the frequency where $\mathrm{Re}\tilde{\epsilon} = 0$. If the crossing occurs at large frequencies (Al, Mg), then the coupling should be small, while if the crossing occurs at low frequencies (transition elements), the coupling should be large.

The infrared properties of the transition elements are characterized by a large frequency-independent dielectric constant ϵ_∞, stemming from many high-frequency interband transitions [see Eq. (5)]. For those metals where $\epsilon_\infty \gg \epsilon_d$ (a condition satisfied by most transition elements), the insulating dielectric overlayer will have minimal influence on the frequency of the electrostatic surface-plasmon frequency ω_s, since now $\omega_s \approx \omega_p/\sqrt{\epsilon_\infty}$, which is also the frequency where $\mathrm{Re}\tilde{\epsilon} = 0$. Without special effort it is unlikely that a distinguishable feature associated with electron–surface-plasmon coupling could be resolved in the optical conductivity of these systems, although a frequency-dependent relaxation time still should be present. This frequency-dependent relaxation parameter need not be the same as was found for the alkali metals.

To fit the far-infrared frequency-dependent relaxation parameter of lead in the strong electron-phonon coupling limit, Allen[22] found that it was necessary to ignore the $(1 - \cos\theta)$ factor in the calculation of the relaxation time. If the same assumption is made here for the electron-surface-plasmon coupling model, then at infrared frequencies the relaxation parameter becomes $[\omega\tau(\omega)]^{-1} \sim \omega$; the same infrared frequency depen-

dence which has been observed for many transition elements.[30-32]

In conclusion, the electron–surface-plasmon absorption process which is an intrinsic phenomenon associated with smooth metal surfaces explains the experimental infrared and optical data on Na, K, and Rb. In particular, the infrared mass enhancement is a natural consequence of the frequency-dependent scattering process. No doubt, interband transitions still occur, but the room temperature optical matrix element must be much smaller than previously calculated. A careful study of the optical properties of selected clean metal surfaces with a variety of dielectric overlayers should provide detailed information on the surface dynamics of this spatially inhomogeneous surface-plasmon coupling process.

ACKNOWLEDGMENTS

Discussions with N. W. Ashcroft, P. Garik, G. Graham, J. W. Wilkins, and R. H. Silsbee have been particularly helpful. A stimulating conservation with A. Overhauser at the Aspen Center for Physics is also acknowledged. Thanks are due to S. Yu for writing the computer programs and to M. Boriack for calling Ref. 6 to my attention. This work was supported by the National Science Foundation through Grant No. DMR-76-81083A02 to the Cornell Materials Science Center.

APPENDIX A

The Wilson-Butcher expression for the interband contribution associated with the 110 reciprocal-lattice vectors in the alkali metals is[11]

$$\sigma_I(\omega)=\begin{cases}\dfrac{me^2}{\pi\hbar^4}\dfrac{|V_{110}|^2}{G_{110}}\dfrac{(\omega_h-\omega)(\omega-\omega_l)}{\omega^3}, & \omega_l<\omega<\omega_h\\ 0 \quad (\omega>\omega_h \text{ and } \omega<\omega_l), & \end{cases} \tag{A1}$$

where G_{110} is the reciprocal-lattice vector and V_{110} is the corresponding Fourier component of the pseudopotential. The low- and high-frequency thresholds are ω_l and ω_h, respectively.

The Kramers-Kronig transform of $4\pi\sigma_I(\omega)/\omega$, namely $\epsilon_{1I}(\omega)$, is

$$\begin{aligned}\epsilon_{1I}(\omega)=\frac{8me^2|V_{110}|^2}{\pi\hbar^4 G_{110}\omega^4}\Bigg\{&\omega^2\left[\ln\left(\frac{\omega_h}{\omega_l}\right)-\frac{\omega_h^2-\omega_l^2}{2\omega_h\omega_l}\right]\\&+\omega_l\omega_h\ln\left(\frac{\omega_h}{\omega_l}\right)\\&-\tfrac{1}{2}(\omega_l-\omega)(\omega_h-\omega)\ln\left|\frac{\omega_h-\omega}{\omega_l-\omega}\right|\\&-\tfrac{1}{2}(\omega_l+\omega)(\omega_h+\omega)\ln\left(\frac{\omega_h+\omega}{\omega_l+\omega}\right)\Bigg\}.\end{aligned} \tag{A2}$$

APPENDIX B

From Ref. 22, the frequency-dependent mass parameter is

$$\bar\lambda(\omega)=-\frac{2}{\omega}\int_0^{\omega_D}d\Omega\,\alpha_{\rm ir}^2F(\Omega)\left(\ln\left|\frac{\omega-\Omega}{\omega+\Omega}\right|-\frac{\Omega}{\omega}\ln\left|\frac{\omega^2-\Omega^2}{\Omega^2}\right|\right), \tag{B1}$$

where ω_D is the maximum phonon frequency of the lattice.

If $\alpha_{\rm ir}^2F(\Omega)$ is given by Eq. (21), where ω_m is the maximum surface-plasmon frequency, then Eq. (B1) gives

$$\bar\lambda(\omega)=\bar\lambda(0)\left\{\frac{3}{4}\left(\frac{\omega_m}{\omega}\right)\left[1-\frac{1}{5}\left(\frac{\omega}{\omega_m}\right)^4\right]\ln\left|\frac{\omega+\omega_m}{\omega-\omega_m}\right|+\frac{1}{10}+\frac{3}{10}\left(\frac{\omega}{\omega_m}\right)^2+\frac{3}{5}\left(\frac{\omega_m}{\omega}\right)^2\ln\left|\frac{\omega_m^2-\omega^2}{\omega_m^2}\right|\right\}, \tag{B2}$$

where

$$\bar\lambda(0)=(20/3\pi)[\omega_m\bar\tau(\omega_m)]^{-1}. \tag{B3}$$

The Kramers-Kronig transform of Eq. (23) gives

$$K[\omega\bar\tau(\omega)]^{-1}=\frac{3\bar\lambda(0)}{10}\left\{\frac{\omega_m}{2\omega}\left[1-\left(\frac{\omega}{\omega_m}\right)^4\right]\ln\left|\frac{\omega+\omega_m}{\omega-\omega_m}\right|+\frac{1}{3}+\left(\frac{\omega}{\omega_m}\right)^2\right\}. \tag{B4}$$

The scaling factor between Eqs. (B2) and (B4) is approximately 2.5, i.e.,

$$\bar\lambda(0)=2.5\lim_{\omega\to0}\{K[\omega\bar\tau(\omega)]^{-1}\}. \tag{B5}$$

APPENDIX C

Following Ref. 25, let the interface plane be at $z=0$ between vacuum $z<0$ and the metal $z>0$, then the surface-plasmon vector potential at the point $\vec r=(\rho,z)$ in the metal is

$$\vec A_{\rm sp}(\vec r)=\sum_{\vec\kappa}\left(\frac{4\pi\hbar c}{L^2P_\kappa}\right)^{1/2}\left(\frac{i\hat\kappa-\hat z\kappa}{\nu}\right)e^{-\nu z+i\vec\kappa\cdot\vec\rho}\times(a_{\vec\kappa}+a_{-\vec\kappa}^\dagger). \tag{C1}$$

Here

$$P_\kappa=[(\epsilon^4-1)/\epsilon^2][-(\epsilon+1)]^{1/2}, \tag{C2}$$

$$\epsilon=1-(\omega_p/\omega_{\vec\kappa})^2, \tag{C3}$$

$$\nu^2=\kappa^2-(\omega_\kappa^2-\omega_p^2)/c^2, \tag{C4}$$

and $\omega_{\vec\kappa}$ is the surface-plasmon eigenfrequency corresponding to a surface plasmon with wave vector κ. The eigenfrequency wave number relation for a vacuum-metal interface is

$$\kappa^2=(\omega/c)^2\epsilon/(1+\epsilon). \tag{C5}$$

[1]A comprehensive presentation of the alkali-metal data through 1973 has been given by P. O. Nilsson, in *Solid State Physics*, edited by H. Ehrenreich, F. Seitz, and D. Turnbull (Academic, New York, 1974), Vol. 29, p. 149.

[2]An updated review of the experimental situation for alkali metals has been given by R. Rouard, Thin Solid Films 34, 303 (1976).

[3]J. Monin and G. A. Boutry, Phys. Rev. B 9, 1309 (1974).

[4]H. Mayer and M. H. el Naby, Z. Phys. 174, 289 (1963).

[5]H. Mayer and B. Hietel, in *Optical Properties and Electronic Structure of Metals and Alloys*, edited by F. Abeles (North-Holland, Amsterdam, 1966), p. 47.

[6]A. W. Overhauser and N. R. Butler, Phys. Rev. B 14, 3371 (1976).

[7]J. Monin, G. Hincelin, and G. A. Boutry, C. R. Acad. Sci. Ser. B 272, 761 (1971).

[8]R. E. Palmer and S. E. Schnatterly, Phys. Rev. B 4, 2329 (1971).

[9]O. Hunderi, Phys. Rev. B 7, 3419 (1973). The wavelength of the E and M wave in the metal, i.e., the skin depth, is comparable to the grain-boundary dimensions so the scattering cross section for the plasmon resonance is much larger than the absorption cross section. The Maxwell-Garnett model presented in this reference is valid only in the opposite limit, i.e., when the grain size is much smaller than the effective wavelength in the medium.

[10]T. Inagaki, L. C. Emerson, E. T. Arakawa, and M. W. Williams, Phys. Rev. B 13, 2305 (1976).

[11]N. V. Smith, Phys. Rev. 183, 634 (1969).

[12]B. Hietel and H. Mayer, Z. Phys. 264, 21 (1973).

[13]N. V. Smith, Phys. Rev. B 2, 2840 (1970).

[14]T. Holstein, Phys. Rev. 96, 535 (1954); Ann. Phys. (N.Y.) 29, 410 (1964).

[15]M. H. Cohen, Philos. Mag. 3, 762 (1958).

[16]J. N. Hodgson, J. Phys. Chem. Solids 24, 1213 (1963).

[17]A. J. Sievers, J. Opt. Soc. Am. 68, 1505 (1978).

[18]S. Roberts, Phys. Rev. 114, 104 (1959), and references therein.

[19]A. H. Wilson, *The Theory of Metals* (Cambridge University Press, New York, 1936), p. 133.

[20]P. N. Butcher, Proc. Phys. Soc. London A64, 50 (1951).

[21]D. J. Stevenson, Phys. Rev. B 7, 2348 (1973).

[22]P. B. Allen, Phys. Rev. B 3, 305 (1971).

[23]R. H. Ritchie, Surf. Sci. 34, 1 (1973).

[24]E. Burstein, W. P. Chen, Y. J. Chen, and A. Harstein, J. Vac. Sci. Technol. 11, 1004 (1974).

[25]J. M. Elson and R. H. Ritchie, Phys. Rev. B 4, 4129 (1971).

[26]I. Inagaki, E. T. Arakawa, R. D. Bukhoff, and M. W. Williams, Phys. Rev. B 13, 5610 (1976).

[27]J. C. Inkson, J. Phys. C 8, L164 (1975).

[28]U. S. Whang, E. T. Arakawa, and T. A. Callcott, Phys. Rev. 6B, 2109 (1972).

[29]W. Y. Ching and J. Callaway, Phys. Rev. Lett. 30, 441 (1973).

[30]J. J. Hopfield, in *Proceedings of the Conference on Superconductivity in d- and f-Band Metals*, edited by D. H. Douglass (A.I.P., New York, 1972), p. 358.

[31]S. R. Nagel and S. E. Schnatterly, Phys. Rev. B9, 1299 (1974).

[32]W. E. Pickett and P. B. Allen, Phys. Rev. B 13, 1473 (1976).

[33]*American Institute of Physics Handbook*, 3rd ed., edited by D. E. Gray (McGraw-Hill, New York, 1972).